Modeling diffractive optical elements for optical data storage applications

Masud Mansuripur

Masud Mansuripur, "Modeling diffractive optical elements for optical data storage applications," Proc. SPIE 6620, Optical Data Storage 2007, 66200N (11 July 2007); doi: 10.1117/12.738645

Event: Optical Data Storage 2007, 2007, Portland, OR, United States

Modeling Diffractive Optical Elements for Optical Data Storage Applications

Masud Mansuripur

College of Optical Sciences, The University of Arizona, Tucson, Arizona 85721
masud@optics.arizona.edu

Abstract. A combination of ray-tracing and diffraction theory is used to model the diffractive optical elements used in optical data storage systems. Details of the theoretical model and some numerical simulation results are presented.

1. Introduction. Optimal design of advanced optical pickups and media requires a thorough understanding of the interaction between the light beam and the various system components located between the laser and the detectors. In this paper we use a combination of polarization ray-tracing and quasi-vector diffraction modeling to analyze the behavior of the laser beam as it propagates through various Diffractive Optical Elements (DOEs).

2. Transmissive Diffractive Optical Element. Figure 1(a) shows a geometric-optical ray (vacuum wavelength = λ_o) arriving through a medium of refractive index n_1 at the surface of a substrate (refractive index = n_2) coated with a variable thickness layer; the angle and the azimuth of incidence are θ_1, ϕ_1, those of the transmitted ray are θ_2, ϕ_2. The incident wavefront at the front facet of the substrate may be written as $A(x, y) = A_o \exp[i(2\pi n_1/\lambda_o)(x\sigma_x + y\sigma_y)]$, where $\sigma_x = \sin\theta_1 \cos\phi_1$ and $\sigma_y = \sin\theta_1 \sin\phi_1$.

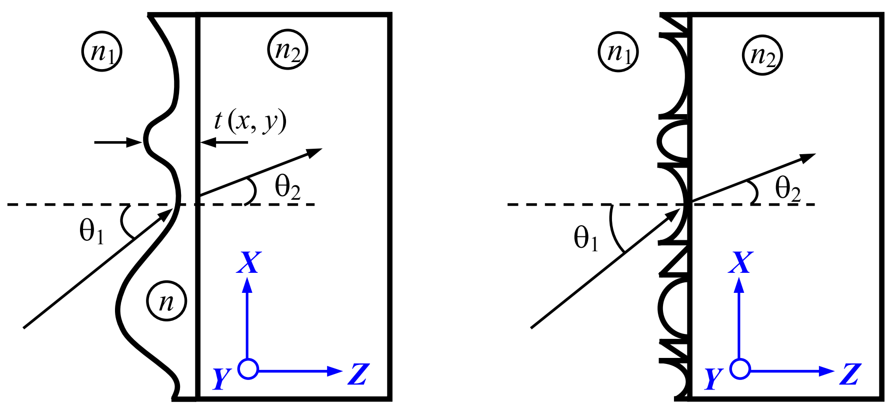

Figure 1. (a) A ray of light (vacuum wavelength = λ_o) is incident at an oblique angle (θ_1, ϕ_1) from a medium of refractive index n_1 onto a substrate of index n_2. The substrate is coated with a layer of index n and variable thickness $t(x, y)$, where n is assumed to be large and $t(x, y)$ very small, so that only the optical path difference, OPD = $(n - n_1)\, t(x, y)$, has a finite value. (b) The variable thickness layer is converted to a DOE by reducing the coating layer's thickness wherever the OPD contains an integer multiple of the construction wavelength λ_c. The characteristic function of the DOE is thus the fractional part $f(x, y)$ of the characteristic function of the coating layer in (a), defined as $F(x, y) = (n - n_1)\, t(x, y)/\lambda_c$.

The coating layer has thickness $t(x, y)$ and refractive index n. To avoid certain complications in the following analysis we shall assume that n is very large and $t(x, y)$ very small, so that only the product $(n - n_1)\, t(x, y)$, known as the optical path difference (OPD), has a finite value. The characteristic function of the coating layer is thus the dimensionless function $F(x, y) = (n - n_1)\, t(x, y)/\lambda_c$, where λ_c is some fixed "construction wavelength." The characteristic function is generally specified by a polynomial such as

Optical Data Storage 2007, edited by Bernard Bell, Takeshi Shimano
Proc. of SPIE Vol. 6620, 66200N, (2007) · 0277-786X/07/$18 · doi: 10.1117/12.738645

$$F(x,y)=\sum_{m=0}^{N}\sum_{n=0}^{N-m} a_{mn}\, x^m y^n. \tag{1a}$$

$F(x, y)$ must be greater than or equal to zero across the surface since $n-n_1$, $t(x, y)$ and λ_c are all non-negative. For later reference, the gradient of $F(x, y)$ is written below:

$$\nabla F(x,y)=(\partial F/\partial x, \partial F/\partial y)=\Big[\sum_{m=1}^{N} m\Big(\sum_{n=0}^{N-m} a_{mn}\, y^n\Big)x^{m-1},\ \sum_{n=1}^{N} n\Big(\sum_{m=0}^{N-n} a_{mn}\, x^m\Big)y^{n-1}\Big]. \tag{1b}$$

A Diffractive Optical Element (DOE) is constructed from the above coating layer by reducing the layer's thickness whenever $F(x, y)$ happens to be greater than unity. By removing from $t(x, y)$ all integer multiples of $\lambda_c/(n-n_1)$, one obtains a coating such as that in Fig. 1(b), for which the integer part of $F(x, y)$, if any, has been eliminated in all locations. The characteristic function $f(x, y)$ of the DOE, with values confined to the interval [0, 1], is simply the fractional part of $F(x, y)$.

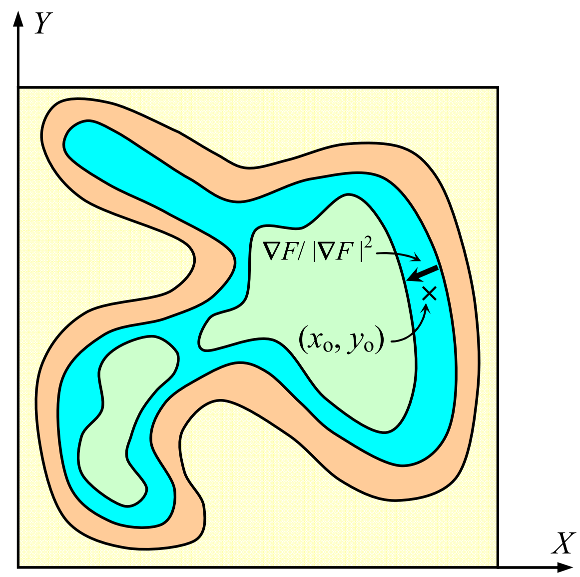

Figure 2. Diagram of a DOE showing the slicing contours where the function $F(x, y)$ assumes integer values. The DOE's characteristic function $f(x, y)$ is the fractional part of $F(x, y)$. Thus, while $F(x, y)$ is continuous across the XY-plane, $f(x, y)$ jumps by one unit at each contour. The space between each pair of adjacent contours contains a single groove of the DOE, where $f(x, y)$ varies continuously between the values of 0 and 1. At an arbitrary location (x_o, y_o) in the XY-plane, the separation between adjacent contours is given by $(\Delta x, \Delta y) = \nabla F/|\nabla F|^2$, which is a vector of magnitude $1/|\nabla F|$ oriented orthogonal to the contours.

As shown in Fig. 2, the coating layer's $F(x, y)$ is truncated at contours where the function acquires integer values, so the local period $(\Delta x, \Delta y)$ of the DOE at a point such as (x_o, y_o) is the shortest line segment through (x_o, y_o) that satisfies the equation

$$\nabla F(x,y)\cdot(\Delta x\,\hat{\boldsymbol{x}}+\Delta y\,\hat{\boldsymbol{y}})=(\partial F/\partial x)\,\Delta x+(\partial F/\partial y)\,\Delta y=1. \tag{2}$$

In Eq. (2) $\hat{\boldsymbol{x}}$ and $\hat{\boldsymbol{y}}$ are unit vectors along the coordinate axes. Noting that $|\nabla F|^2=(\partial F/\partial x)^2+(\partial F/\partial y)^2$, we find $(\Delta x, \Delta y) = \nabla F/|\nabla F|^2$. This is the local period of the grating at (x_o, y_o), which is directed along ∇F and has magnitude $1/|\nabla F|$. In the linear approximation, a single period of the grating begins at $(x, y)=(x_o, y_o)-f(x_o, y_o)\nabla F/|\nabla F|^2$, where $f(x, y) = 0$, and ends at $(x, y) = (x_o, y_o) + [1-f(x_o, y_o)]\,\nabla F/|\nabla F|^2$, where $f(x, y) = 1$.

Since n is assumed to be large, inside the coating layer of Fig. 1(a) the ray travels along the Z-axis and acquires an extra phase $\Psi(x, y) = 2\pi(n - n_1)\, t(x, y)/\lambda_o = 2\pi(\lambda_c/\lambda_o)F(x, y)$. As long as $\lambda_o = \lambda_c$, the truncation of $F(x, y)$, i.e., removal of its integer part, does not affect the acquired phase shift $\Psi(x, y)$; in other words, eliminating 2π multiples does not change the transmitted beam's phase profile. However, when $\lambda_o \neq \lambda_c$, the XY-plane may be divided into segments, defined by the contours of truncation, where the phase of the transmitted beam over each segment differs from $\Psi(x, y)$ by some integer-multiple of $2\pi(\lambda_c/\lambda_o)$; the DOE thus modulates the incident phase by $\psi(x, y) = 2\pi(\lambda_c/\lambda_o) f(x, y)$. In the vicinity of an arbitrary point (x_o, y_o), considering the local periodicity of the grating along the direction ∇F, the modulating phase function $\exp[i\psi(x, y)]$ may be expanded in the following (one-dimensional) Fourier series:

$$\exp[i2\pi(\lambda_c/\lambda_o) f(x, y)] = \sum_m C_m \exp\{i2\pi m[(\partial F/\partial x)(x - x_o) + (\partial F/\partial y)(y - y_o)]\}, \tag{3a}$$

where the Fourier coefficients are given by

$$C_m = |\nabla F| \int \exp[i2\pi(\lambda_c/\lambda_o) f(x, y)] \exp(-i2\pi m|\nabla F|\, s)\, ds. \tag{3b}$$

In Eq.(3b), the one-dimensional integral is taken in the XY-plane along a straight line segment drawn parallel to ∇F through (x_o, y_o); the range of integration, starting at $(x, y) = (x_o, y_o) - f(x_o, y_o)\nabla F/|\nabla F|^2$ and ending at $(x, y) = (x_o, y_o) + [1 - f(x_o, y_o)]\,\nabla F/|\nabla F|^2$, covers one full period of the grating; see Fig. 2. Expanding $f(x, y)$ to first order in Taylor series yields

$$f(x, y) = f(x_o, y_o) + (\partial F/\partial x)(x - x_o) + (\partial F/\partial y)(y - y_o). \tag{4}$$

Substituting for $f(x, y)$ in Eq.(3b) from Eq.(4) and carrying out the integration, we find

$$C_m = \exp[i2\pi m f(x_o, y_o)] \exp\{i\pi[(\lambda_c/\lambda_o) - m]\}\, \mathrm{sinc}[(\lambda_c/\lambda_o) - m], \tag{5}$$

where $\mathrm{sinc}(x) = \sin(\pi x)/\pi x$. The m^{th} order diffraction efficiency is thus found to have the constant amplitude $|C_m| = \mathrm{sinc}[(\lambda_c/\lambda_o) - m]$ across the XY-plane for any given λ_o. When λ_o happens to be the same as the construction wavelength λ_c, the first order beam will have 100% efficiency while all other orders vanish. Also, if λ_c is an integer-multiple of λ_o, only one order will emerge, unattenuated, from the DOE. For all other values of λ_o, the various orders $m = 0, \pm 1, \pm 2$, etc., will coexist. The second term in Eq.(5) corresponds to a constant phase, $\pi[(\lambda_c/\lambda_o) - m]$, which is independent of (x_o, y_o) and may thus be ignored in practice. The remaining phase, $2\pi m f(x_o, y_o)$, varies continuously across the XY-plane with absolutely no dependence on λ_o. Since $f(x_o, y_o)$ is the fractional part of $F(x_o, y_o)$, the two functions may be exchanged and the phase acquired by the m^{th} order rays written as $2\pi m F(x_o, y_o)$. In practice the lack of any discontinuous jumps in this phase profile of the m^{th} order beam is extremely important, since it means that the wavefront associated with each and every diffraction order is well-behaved. In other words, if one assembles all the m^{th} order rays from across the DOE to construct the m^{th} order transmitted beam, the beam will have a continuous wavefront.

The transmitted wavefront around (x_o, y_o), the foot of the incident ray, can now be written

$$A(x, y) = \sum_m A'_m \exp[\mathrm{i}\,(2\pi n_2/\lambda_o)\,(x\sigma'_{xm} + y\sigma'_{ym})]$$

$$= A_o \exp[\mathrm{i}\,(2\pi n_1/\lambda_o)\,(x\sigma_x + y\sigma_y)]\,\exp[\mathrm{i}\,\psi(x, y)]$$

$$= \sum_m C_m A_o \exp\{\mathrm{i}\,(2\pi/\lambda_o)\,[(n_1\sigma_x + m\lambda_o\partial F/\partial x)\,x + (n_1\sigma_y + m\lambda_o\partial F/\partial y)\,y]\}. \quad (6)$$

The (complex) amplitude and the direction of the m^{th} order transmitted ray are thus given by

$$A'_m = C_m A_o, \quad (7a)$$

$$(\sigma'_x, \sigma'_y)_m = (n_1\sigma_x + m\lambda_o\partial F/\partial x,\ n_1\sigma_y + m\lambda_o\partial F/\partial y)\,/n_2. \quad (7b)$$

Note that the mismatch between the refractive indices n_1, n, and n_2 is not taken into consideration in Eq.(7a) as far as reflection losses at the various interfaces are concerned. Also ignored in this analysis are the effects of incident polarization on the transmission coefficient C_m, which would have required a rigorous vector diffraction treatment.

For $m \neq 0$, the direction of the m^{th} order transmitted ray, $(\sigma'_x, \sigma'_y)_m$, is seen from Eq.(7b) to depend on the illumination wavelength λ_o in a way that gives rise to a substantial amount of chromatic aberration; this provides the basis for correcting the chromatic aberrations of conventional refractive lenses by incorporating diffractive optical elements in the so-called hybrid designs. In going from medium 1 to medium 2 of Fig. 1, the undiffracted 0^{th} order ray follows the Snell's law since, according to Eq.(7b), $(n_2\sigma'_{xo}, n_2\sigma'_{yo}) = (n_1\sigma_x, n_1\sigma_y)$. For other diffraction orders, one must add $m\lambda_o\nabla F$ to the incident beam's $(n_1\sigma_x, n_1\sigma_y)$ in order to obtain the transmitted beam's $(n_2\sigma'_x, n_2\sigma'_y)_m$.

Having exploited the localized ray picture to build the transmitted wavefront(s) across the DOE surface, we now abandon the rays and concentrate instead on the transmitted wavefronts (one for each diffracted order). When the incident wavelength λ_o differs from the construction wavelength λ_c, the various orders will be present in the mix in different amounts, with the magnitude of the m^{th} beam, $|C_m|$, being a function of m and the wavelength ratio λ_c/λ_o. Although the phase profile of each diffracted order is independent of the incident wavelength λ_o, this does *not* imply that a given diffracted order behaves identically in response to different incident wavelengths. Remember that the m^{th} order phase profile is $\exp[\mathrm{i}2\pi mF(x, y)]$, so, for simplicity's sake, let us assume that $F(x, y) = \alpha x + \beta y$, where α and β are arbitrary constants. This phase profile may then be written as $\exp[\mathrm{i}(2\pi/\lambda)(m\lambda\alpha x + m\lambda\beta y)]$, where $\lambda = \lambda_o/n_2$ is the wavelength within the medium of refractive index n_2. This represents a plane wave having direction cosines $(\sigma_x, \sigma_y) = (m\lambda\alpha, m\lambda\beta)$, whose propagation direction evidently depends on λ_o, even though its phase profile is independent of the incident wavelength. The bottom line is that the rays and the wavefronts that emerge from the above analysis paint a consistent picture, both leading to the same conclusions concerning the diffraction efficiency and the chromatic aberrations associated with each diffracted order of the transmitted beam.

3. Reflective Diffractive Optical Element. The arguments of the preceding section may be extended to cover the case of an ideal reflective DOE shown in Fig. 3. As before, the incidence medium has refractive index n_1, but the DOE's substrate is a perfect reflector. We assume once again that the variable-thickness layer has a large refractive index n and a correspondingly small thickness $t(x, y)$. The optical path difference upon transmission through the layer and reflection at the substrate interface is thus given by $\mathrm{OPD} = 2(n-n_1)\,t(x, y)$, which yields the characteristic function $F(x, y) = 2(n-n_1)\,t(x, y)/\lambda_c$, with λ_c being the construction wavelength. Once again, the DOE is constructed from the above coating layer by reducing the layer's thickness whenever $F(x, y)$ exceeds unity. Note that the above factor of 2 in the expression for the OPD – representing the effect of double-path through the coating layer – does not affect any of the subsequent results, since the starting point of our derivations is the function $F(x, y)$, which already incorporates this factor. The formal derivations for a reflective DOE parallel those of the transmissive DOE in the preceding section, until we reach Eq.(6), at which point the refractive index n_2 of the medium into which the beam emerges (upon transmission through the DOE) must be replaced with n_1, reflecting the fact that the incidence and emergence media are now the same. Therefore, for reflective DOEs, the only equation that needs to be modified is Eq.(7b), which assumes the following form:

$$(\sigma'_x, \sigma'_y)_m = \left[\sigma_x + (m\lambda_o/n_1)\,\partial F/\partial x,\ \sigma_y + (m\lambda_o/n_1)\,\partial F/\partial y\right]. \tag{8}$$

All the considerations discussed in the case of transmissive DOEs apply equally to reflective elements as well.

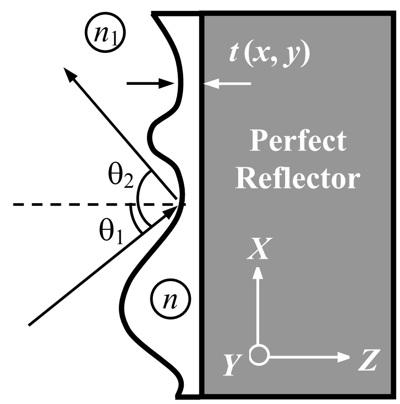

Figure 3. The case of a reflective DOE differs from that of a transmissive DOE in that the transparent substrate is now replaced with a perfect reflector. The incident rays, after traveling through the coating layer, bouncing back at the substrate interface, and returning through the same thickness of the coating layer, re-emerge into the incidence medium (refractive index = n_1). The DOE is constructed from the coating layer by removing from $t(x, y)$ all integer multiples of $\frac{1}{2}\lambda_c/(n - n_1)$.

4. DOE on a curved surface. Curved surfaces may also be coated with DOEs, and the method of calculating reflected/transmitted rays is essentially the same as that described in conjunction with flat surfaces in the preceding sections. The reason is that all such calculations are based on the properties of the surface and of the incident and emergent rays over small patches, where curved surfaces are flat locally. The only complication arises from the fact that the DOE's characteristic function is usually defined with respect to a coordinate system whose axes do not follow the profile of the surface. We limit the present discussion to the case of a curved surface of revolution, such as that in Fig. 4, where the axis of symmetry is z, and the sag is a given function $h(r)$ of r. The characteristic function of such a DOE is usually defined by a radial polynomial,

$$F(r) = \sum_{n=0}^{N} a_n r^n. \tag{9}$$

Consider the local surface coordinate s shown in Fig. 4. The value of s at each point on the surface is the length of the curve measured from some point of reference such as the vertex at $(r, z) = (0, 0)$. What we need is the characteristic function's gradient over a short distance Δs, namely, $\Delta F/\Delta s$. But

$$\Delta s = \sqrt{(\Delta r)^2 + (\Delta h)^2} = \Delta r\ \sqrt{1 + (\mathrm{d}h/\mathrm{d}r)^2}\,. \tag{10}$$

Therefore,

$$\partial F/\partial s = (\partial F/\partial r)/\sqrt{1 + (\mathrm{d}h/\mathrm{d}r)^2} \tag{11}$$

Equation (11), in conjunction with the equations derived previously for flat surfaces, is all that one needs in order to compute the various diffracted rays and wavefronts associated with DOEs on curved substrates.

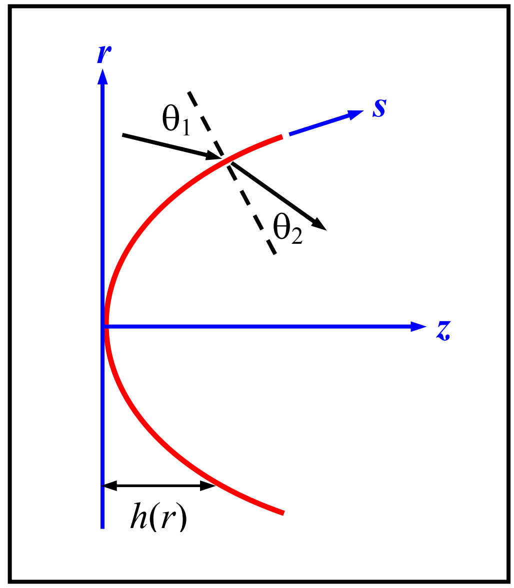

Figure 4. A surface of revolution around the z-axis is defined by its sag $h\,(r)$, which is the distance of the surface (along z) from the plane tangent to the surface at its vertex. The curvilinear coordinate s follows the tangent to the surface in the $r\,z$-plane. The value of s at each point is the length of the curve measured from some point of reference, such as the vertex at $(r, z) = (0, 0)$. Also shown is a pair of incident and refracted rays at the surface.

5. Transmissive DOE sandwiched between a pair of flat substrates. Figure 5 shows an aspheric lens illuminated with a Gaussian beam ($\lambda_o = 0.66\mu$m, e^{-1} radius $R_o = 2.5$mm, diameter $D = 4.0$mm). The emerging convergent beam passes through a glass plate on its way to a flat DOE sandwiched between a substrate and a cover slip. The DOE's construction wavelength λ_c is the same as λ_o (hence the emergent beam is the +1st diffracted order), and its phase profile is given by (x and y in millimeters):

$$F(x, y) = 639.77x + 17.47x^2 - 19.76\,y^2 - 30.18\,x^3 - 0.0042\,x^2 y - 33.69\,xy^2 + 0.0021\,y^3 - 3.25\,x^4.$$

The incident rays are traced through the entire system, then back traced to the so-called destination plane, located at $z = 10$ mm from the first vertex of the lens and tilted by $\theta = 6.03°$, as shown. At the destination plane, the magnitude, phase, and polarization state of the rays are used to reconstruct the wavefront. Figure 6 shows the reconstructed wavefront's intensity and phase distribution at the destination plane. The wavefront's curvature and tilt are factored out, otherwise the phase variations across the cross-sectional profiles will be too great to display. Note that the y-component is nearly four orders-of-magnitude weaker than the x-component, whereas the z-component's power content is non-negligible. The phase profiles of Fig. 6 are quite uniform, corresponding to a small residual aberration with an r.m.s. wavefront error $\approx 0.003\lambda_o$.

Figure 7 shows plots of log_intensity, intensity, and phase in the plane of best focus for the *x*-, *y*-, and *z*-components of polarization. Note that the *y*-component is nearly four orders-of-magnitude weaker than the *x*-component, whereas the *z*-component is fairly strong. The observed linear phase profile is due to the 6.03° tilt of the focal plane relative to the incident beam coordinates (see the focal plane coordinates in Fig. 5).

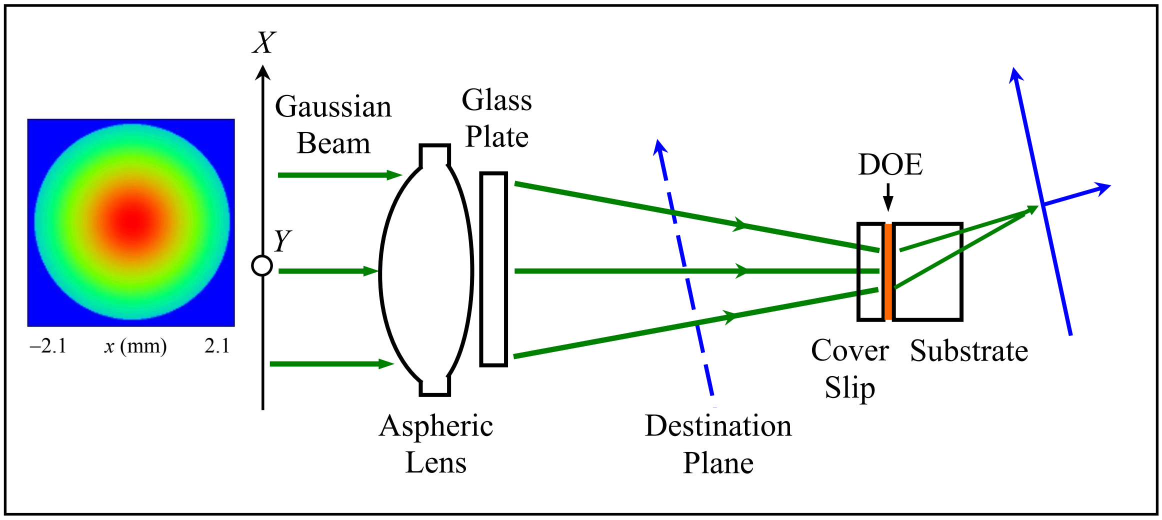

Figure 5. Gaussian beam ($\lambda_o = 0.66\mu$m, e^{-1} radius $R_o = 2.5$mm, diameter $D = 4.0$mm) is focused by a 4.0mm diameter lens (thickness = 1.7 mm, refractive index = 1.54044, first surface: radius of curvature $R_c = 11.4$ mm, conic constant $\kappa = -0.733$, aspheric coefficients $A_4 = 2.82 \times 10^{-7}$, $A_6 = -3.75 \times 10^{-8}$, $A_8 = -1.5 \times 10^{-9}$; second surface: $R_c = -98$ mm). The incident beam, linearly polarized along the *x*-axis, has the intensity profile shown on the left-hand side. The glass plate ($d_1 = 0.61$ mm), the cover slip ($d_2 = 0.5$mm), and the substrate ($d_3 = 2.0$ mm) all have the same refractive index $n = 1.520168$. The glass plate is 1.0 mm away from the lens and 14.38 mm away from the cover slip. The destination plane is at $z = 10.0$ mm (measured from the first vertex of the lens), and is tilted by $\theta = 6.03°$, as shown. The beam is subsequently propagated a distance of 10.468 mm along the normal to the destination plane, which brings the beam to its plane of best focus.

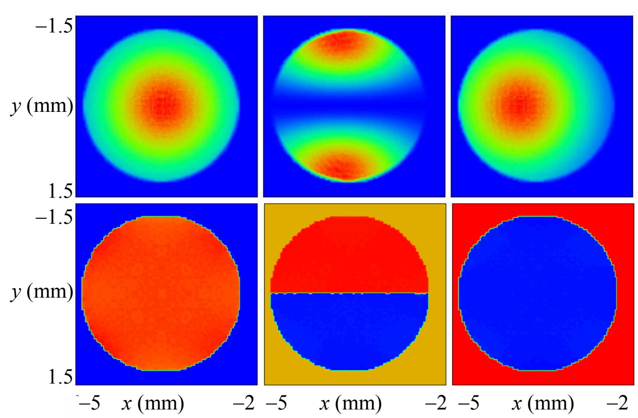

Figure 6. Distributions of intensity (top) and phase (bottom) at the Destination plane in the system of Fig. 5; from left to right, *x*-, *y*-, and *z*-components of polarization. Note that the emergent beam is centered at $x = -3.6$ mm. The peak intensities are in the ratio of $I_x : I_y : I_z = 1.0 : 0.39 \times 10^{-3} : 0.13$. In the residual phase profiles ϕ_x, ϕ_y, ϕ_z, where the wavefront curvature and tilt are factored out, the color spectrum in each plot covers the range from minimum (blue) to maximum (red); here ($\phi_{\min} : \phi_{\max}$) is (0° : 39°) for ϕ_x, (−147° : 39°) for ϕ_y, and (−146° : 0°) for ϕ_z.

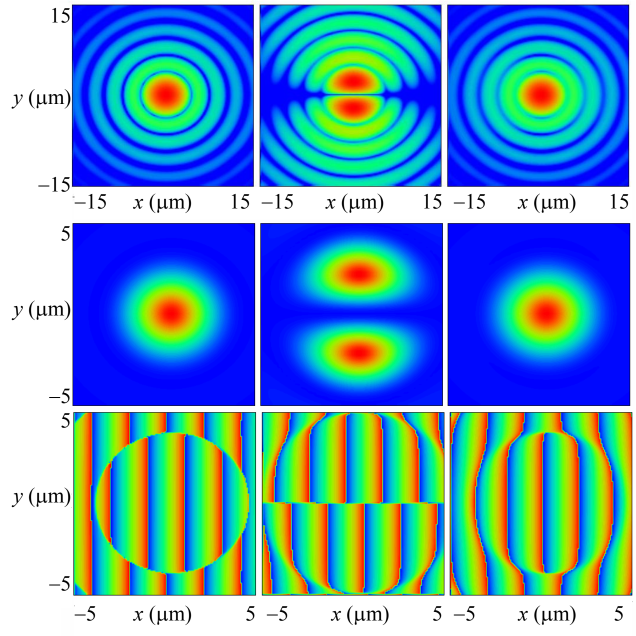

Figure 7. Plots of log_intensity (top), intensity (middle), and phase (bottom) at the plane of best focus in the system of Fig. 5. From left to right: x-, y-, and z-components of polarization. The peak intensities are in the ratio of $I_x : I_y : I_z = 1.0 : 0.15 \times 10^{-3} : 0.115$. The phase profiles' range (blue to red) is $(\phi_{\min} : \phi_{\max}) = (-180° : 180°)$.

6. Reflective DOE on flat substrate. Figure 8 shows a flat DOE on the rear facet of a glass prism, illuminated by a Gaussian beam ($\lambda_o = 0.65\mu\text{m}$, e^{-1} radius $R_o = 2.0\text{mm}$, diameter $D = 3.0\text{mm}$, linearly polarized along x). The only emergent beam is the $+1^{\text{st}}$ diffracted order, as the DOE's construction wavelength λ_c is the same as λ_o. The DOE's aperture diameter is 5.0mm, and its phase profile within its own plane is $F(x, y) = 3.0(x^2 + y^2)$; here both x and y are in millimeters.

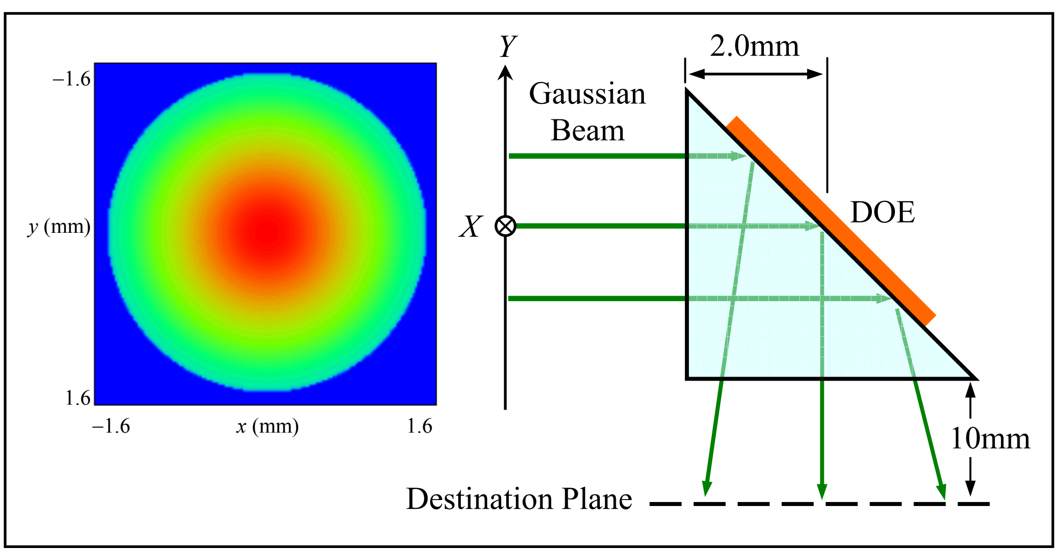

Figure 8. A linearly polarized Gaussian beam enters a glass prism of refractive index $n = 1.65$ whose rear facet is coated with a DOE. The incident beam's intensity profile is shown on the left-hand side. The emergent diffracted beam is the $+1^{\text{st}}$ order. The entrance and exit facets of the prism are antireflection-coated, and the Destination Plane is a distance $\Delta y = 10\text{mm}$ below the prism's exit facet.

Figure 9 shows the reflected intensity and phase profiles at the destination plane. These plots depict intensity (top), phase (middle), and phase_minus_curvature (bottom), with the x, y, z-components of polarization shown from left to right. Note that the y- and z-components are several orders-of-magnitude weaker than the x-component. The DOE's 45° tilt produces the astigmatism seen in the phase plots.

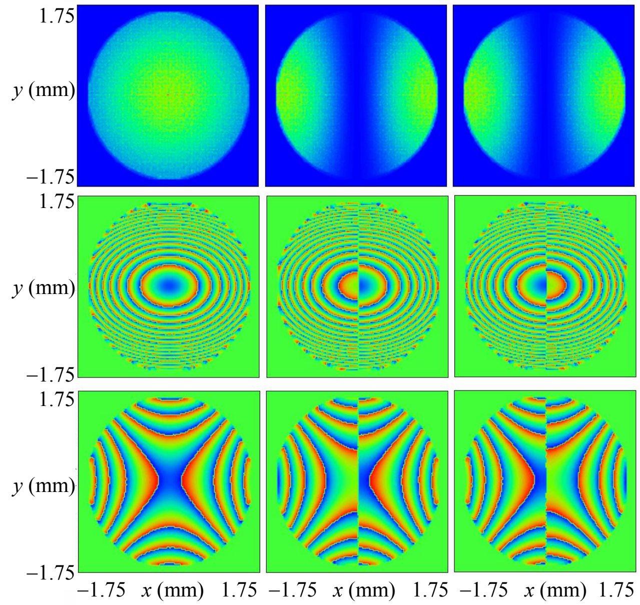

Figure 9. Plots of intensity (top), phase (middle), and phase_minus_curvature (bottom) at the destination plane of the system of Fig. 8. From left to right: x-, y-, and z-components of polarization. The peak intensities are in the ratio of $I_x : I_y : I_z = 10^5 : 0.4 : 1.08$. The range of the phase profiles (blue to red) is $(\phi_{\min} : \phi_{\max}) = (-180° : 180°)$.

7. Transmissive DOE on an aspheric glass lens. Figure 10 shows a DOE-coated aspheric lens illuminated with a Gaussian beam ($\lambda_o = 0.78\mu$m, e^{-1} radius $R_o = 2.0$ mm, diameter $D = 3.0$ mm, linearly polarized along x). The DOE's phase profile is $F(r) = 4.2r^2 - 2.5r^4 + 0.25r^6$ (r in mm), and its construction wavelength λ_c is the same as λ_o; hence the emergent beam is the +1st diffracted order.

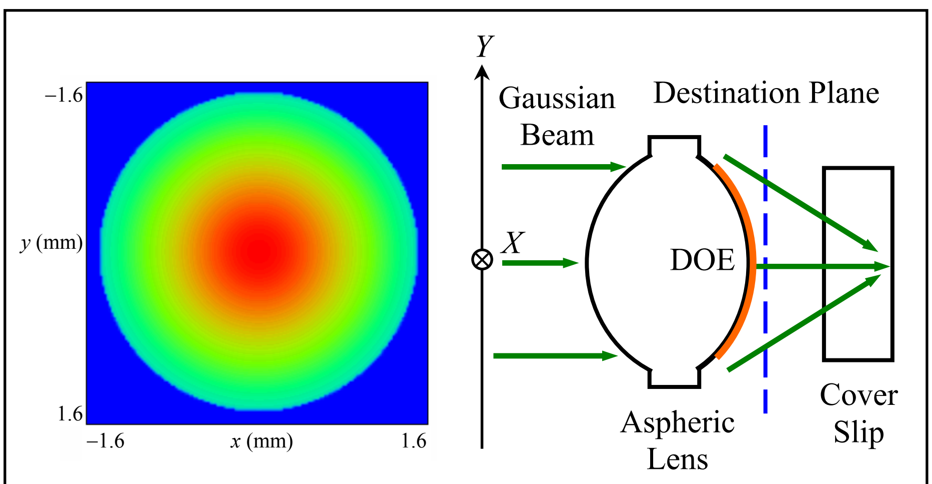

Figure 10. A linearly polarized Gaussian beam is focused via a DOE-coated bi-aspheric lens through a glass cover slip ($d = 1.2$ mm, $n = 1.573456$), which is separated from the lens by 1.0 mm. The incident beam's intensity profile is shown on the left-hand side. The 3 mm diameter lens has thickness = 1.8256 mm, refractive index = 1.597075, first surface parameters: radius of curvature $R_c = 1.93$ mm, conic constant $\kappa = -0.655844$, aspheric coefficients $A_4 = 2.833 \times 10^{-3}$, $A_6 = -4.389 \times 10^{-5}$, $A_8 = 1.524 \times 10^{-4}$; $A_{10} = -1.177 \times 10^{-4}$; and second surface parameters: $R_c = -6.744$ mm, $\kappa = -31.754$, $A_4 = -7.358 \times 10^{-3}$, $A_6 = 2.5077 \times 10^{-3}$, $A_8 = 1.106 \times 10^{-3}$; $A_{10} = -3.871 \times 10^{-4}$. The destination plane is at the exit pupil of the aspheric singlet, and the beam is subsequently propagated to the focal plane.

The incident rays are first traced through the entire system, then back traced to the destination plane located at the exit pupil of the objective lens; the emergent wavefront is subsequently reconstructed from the traced rays. Figure 11 shows plots of intensity and phase at the destination plane. Shown from left to right are the x-, y-, and z-components of polarization. The curvature of the wavefront has been factored out, so what is displayed is the residual phase or aberrations. Note that the y-component is nearly three orders-of-magnitude weaker than the x-component, but the z-component is not so weak. The wavefront at the exit pupil is then propagated to the focal plane and shown in Fig. 12, where the y-component of polarization is seen to be more than three orders-of-magnitude weaker than the x-component.

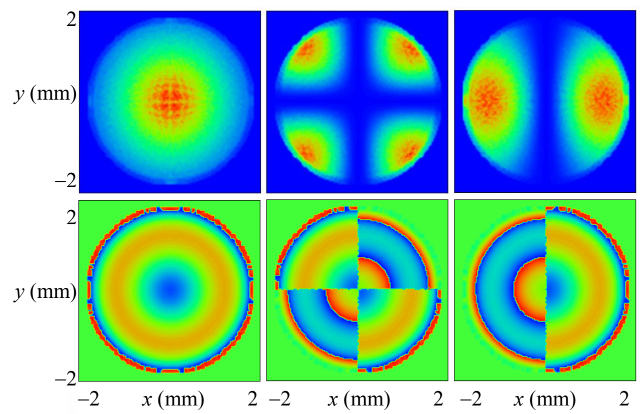

Figure 11. Plots of intensity (top) and phase (bottom) at the exit pupil of the aspheric lens in the system of Fig. 10. From left to right: x-, y-, and z-components of polarization. The peak intensities are in the ratio of $I_x : I_y : I_z = 1000 : 0.6 : 70$. The range of the phase profiles (blue to red) is $(\phi_{\min} : \phi_{\max}) = (-180° : 180°)$.

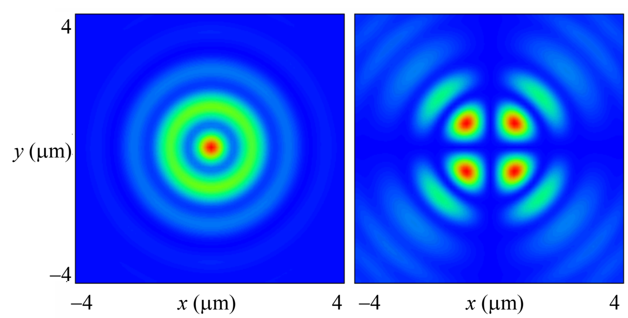

Figure 12. Intensity distribution at the focal plane of the lens in the system of Fig. 10; (left) x-component, (right) y-component of polarization. The peak intensities are in the ratio $I_x : I_y = 1000 : 0.27$.

8. Reflective DOE on a parabolic mirror. Figure 13 shows the diagram of a DOE-coated parabolic mirror illuminated with a Gaussian beam ($\lambda_o = 0.65\mu$m, e^{-1} radius $R_o = 2.0$mm, diameter $D = 3.0$mm, linearly polarized along the x-axis). The paraboloid has radius of curvature $R_c = 40$mm, conic constant $\kappa = -1$, and aperture diameter $D = 3.0$mm; the DOE's phase profile is given by $F_2(r) = r^2 - 1.25r^4 + 0.35r^6 + 0.1r^8$ (r in millimeters). Since the DOE's construction wavelength is $\lambda_c = 0.55\mu$m, various diffracted orders exist, although the most intense beam, shown in Fig. 14, is the $+1^{\text{st}}$ order. Figure 14 shows the reflected intensity and phase profiles at the destination plane, located 10.0 mm away from the mirror's vertex; this also happens to be 10.0 mm before the mirror's nominal focal plane. From left to right, these plots represent the x-, y-, and z-components of polarization. Note that the y-component is nearly six orders-of-magnitude weaker than the x-component, whereas the z-component is only ~600 times weaker.

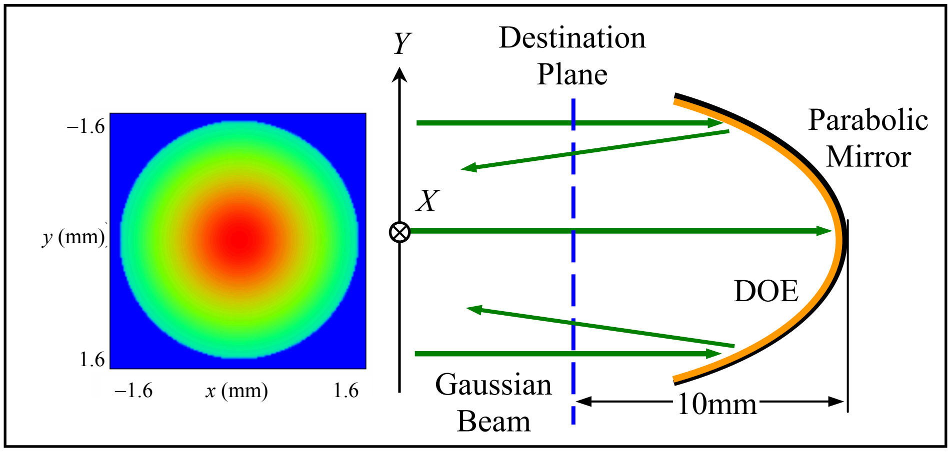

Figure 13. A Gaussian beam is reflected from a DOE-coated parabolic mirror. The incident beam, linearly polarized along the *x*-axis, has the intensity profile shown on the left-hand side. Since the DOE's construction wavelength λ_c is 0.55µm, various diffracted orders exist, although the most intense beam, shown in Fig. 14, is the +1st order. The destination plane is a distance Δz = 10.0 mm from the vertex of the paraboloid.

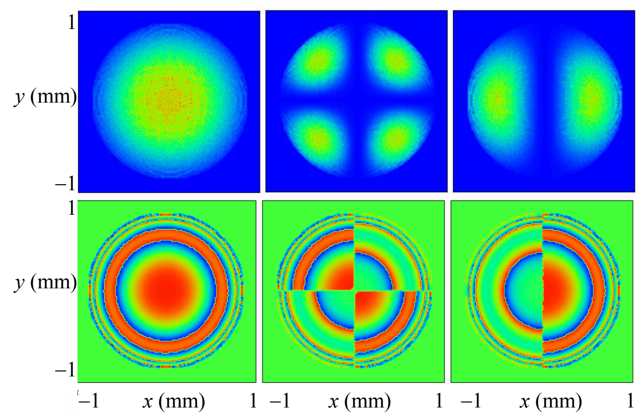

Figure 14. Plots of intensity (top) and phase (bottom) at the destination plane of the system of Fig. 13. From left to right: *x*-, *y*-, and *z*-components of polarization. The peak intensities are in the ratio of $I_x : I_y : I_z$ = $1.0 : 0.33 \times 10^{-6} : 0.177 \times 10^{-2}$. The range of the phase profiles (blue to red) is ($\phi_{\min} : \phi_{\max}$) = (−180° : 180°). For display purposes the curvature phase factor has been taken out of the mesh.

References

1. J. Turunen and F. Wyrowski, *Diffractive Optics for Industrial and Commercial Applications*, Akademie Verlag, Berlin, 1977.
2. W. Veldkamp and T. J. McHugh, "Binary Optics," *Scientific American*, New York, 1992.
3. W. C. Sweatt, "Describing holographic optical element as lens," *J. Opt. Soc. Am.* **67**, 803 (1977).
4. M. W. Farn, "Quantitative comparison of the general Sweatt model for the grating equation," *Appl. Opt.* **31**, 5312 (1992).
5. L. N. Harza, "Kinoform lenses: Sweatt model and phase function," *Optics Communications* **117**, 31 (1995).
6. F. Wyrowski, "Diffractive optical elements: iterative calculation of quantized, blazed phase structures," *J. Opt. Soc. Am. A* **7**, 961 (1990).